SCIENTIFIC REPORTS

OPEN

SUBJECT AREAS:
DRUG DISCOVERY
EXPERIMENTAL MODELS OF DISEASE

Received
17 February 2014

Accepted
7 July 2014

Published
1 August 2014

Correspondence and requests for materials should be addressed to Y.N. (nabemr@lmls-kobe.org)

Calpain 1 inhibitor BDA-410 ameliorates *α-klotho*-deficiency phenotypes resembling human aging-related syndromes

Yoko Nabeshima[1], Miwa Washida[1], Masaru Tamura[2], Akiteru Maeno[2], Mutsuko Ohnishi[3], Toshihiko Shiroishi[2], Akihiro Imura[1], M. Shawkat Razzaque[3,4] & Yo-ichi Nabeshima[1]

[1]Laboratory of Molecular Life Science, Institute of Biomedical Research and Innovation Foundation for Biomedical Research and Innovation 2-2 Minatojima- Minamimachi Chuo-ku, Kobe 650-0047 Japan, [2]Genetic Strains Research Center, Mammalian Genetics Laboratory, National Institute of Genetics, 1111 Yata, Mishima, Shizuoka 411-8540, Japan, [3]Department of Oral Medicine, Infection, and Immunity, Harvard School of Dental Medicine, 190 Longwood Ave, Boston, Massachusetts, USA, [4]Department of Applied Oral Sciences, The Forsyth Institute, 245 First Street, Cambridge, Massachusetts, USA.

Taking good care of elderly is a major challenge of our society, and thus identification of potential drug targets to reduce age-associated disease burden is desirable. *α-klotho*$^{-/-}$ (*α-kl*) is a short-lived mouse model that displays multiple phenotypes resembling human aging-related syndromes. Such ageing phenotype of *α-kl*$^{-/-}$ mice is associated with activation of a proteolytic enzyme, Calpain-1. We hypothesized that uncontrolled activation of calpain-1 might be causing age-related phenotypes in *α-kl*-deficient mice. We found that daily administration of BDA-410, a calpain-1 inhibitor, strikingly ameliorated multiple aging-related phenotypes. Treated mice showed recovery of reproductive ability, increased body weight, reduced organ atrophy, and suppression of ectopic calcifications, bone mineral density reduction, pulmonary emphysema and senile atrophy of skin. We also observed ectopic expression of FGF23 in calcified arteries of *α-kl*$^{-/-}$ mice, which might account for the clinically observed association of increased FGF23 level with increased risk of cardiovascular mortality. These findings allow us to propose that modulation of calpain-1 activity is a potential therapeutic option for delaying age-associated organ pathology, particularly caused by the dysregulation of mineral ion homeostasis.

*α-k*l was identified as a causable gene for a short-lived model mouse that displays numerous morphological features resembling human aging syndromes[1]. On the basis of both macroscopic and histological appearance, *α-kl* $^{-/-}$ mice appears normal until 3 week of age, after which they display growth retardation and body weights remained under 10 g throughout the life spans under standard nutritional and exercise conditions, and die prematurely (average life spans of 77 days). *α-kl*$^{-/-}$ mice display multiple phenotypes that resemble human aging-related syndromes, including atherosclerosis, calcifications in various soft tissues (aorta and artery, lung, kidney, stomach, gut, heart, skin, choroid plexus), malformation of bones with abnormal calcification at the epiphysis and reduced bone density in the diaphysis, kyphosis, pulmonary emphysema, senile atrophy of skin, generalized tissue atrophy, reduction of white fat deposits in all examined organs, and infertility[1,3]. Of particular interest, serum levels of 1,25-$(OH)_2$D in *α-kl*$^{-/-}$ mice were 5 times higher than those of wild type mice at 2 week of age, before the occurrence of multiple histological phenotypes, and remained significantly higher for whole lifespan[2]. Such high serum levels of 1,25-$(OH)_2$D in *α-kl*$^{-/-}$ mice are also associated with dysregulation of serum calcium, phosphate and fibroblast growth factor 23 (FGF23), the major serological phenotypes of *α-kl*$^{-/-}$ mice. More importantly, reducing serum levels of 1,25-$(OH)_2$D in *α-kl*$^{-/-}$ mice, either by dietary restriction[3], or by genetic manipulation[4,5] could improve many of the aging related phenotypes seen in *α-kl*$^{-/-}$ mice, with prolonged survival.

Based on the evidence that the phenotypes of *α-kl* deficient mice largely overlap with those of *Fgf23*-null mice, and that *α-kl* and *Fgf23* double knockout mice have identical phenotype, as their single knockout counterparts[6], a functional crosstalk between α-Kl and FGF23 was proposed[7]. In fact, FGF23 secreted from osteocytes is transported to the kidney, where FGF23 binds to α-Kl, leading to conversion of the canonical FGF receptor 1 (FGFR1)

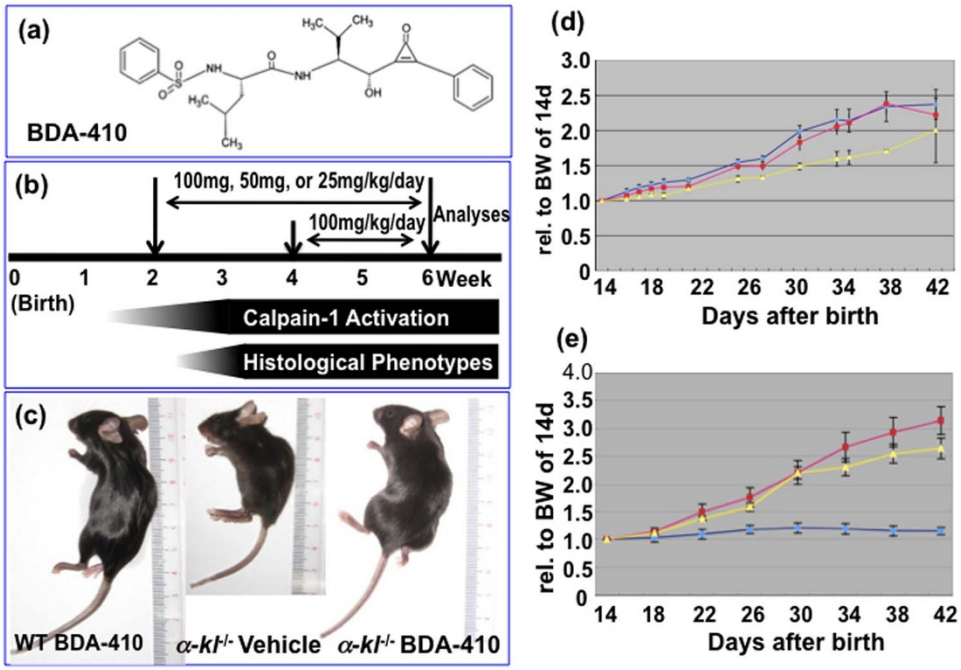

Figure 1 | **Strategies for BDA-410 administration.** (a); Structure of BDA-410, (b); Time course and doses of BDA-410 administration, (c); Gross features of mice, (d); dose-response test, intra-peritoneal administrations of 25 mg/kg/day (yellow, n=4), 50 mg/kg/day (red, n=4) and 100 mg/kg/day (blue, n=4). (e); body weight gains of wild-type (red, 100 mg/kg/day BDA-410, n=7), α-*kl*$^{-/-}$ (blue, vehicle, n=3), and α-*kl*$^{-/-}$ (yellow, 100 mg/kg/day, BDA-410, n=10).

to a receptor specific for FGF23. Subsequent signaling suppresses $1,25(OH)_2D$ activation and decreases phosphate (Pi) reabsorption in the kidney. Therefore, in α-*kl*$^{-/-}$ mice, these two negative signals are impaired and leading to increased serum accumulation of $1,25(OH)_2D$ and Pi, in turn might induce FGF23 synthesis in the bone[8,9].

It is noteworthy that aging-related phenotypes seen in α-*kl*$^{-/-}$ mice are also very similar to many of the complications that develop in patients suffering from advanced-stage of chronic kidney diseases (CKD)[10–14]. This similarity is further supported by evidence that (i) expression of α-*kl* mRNA and α-Kl protein is severely reduced in these patients[15], (ii) high serum phosphate, the major cause of abnormalities of α-*kl*$^{-/-}$ mice, has been reported to be closely associated with high levels of cardiovascular disease morbidity and mortality in patients with CKD, particularly in patients with end-stage renal disease[16–18], and (iii) defects in FGF23[19] and α-Kl[1], together with dysregulation of endogenous anti-calcification factors such as matrix Gla protein, osteoprotegerin, carbonic anhydrase isoenzyme II, fibrillin-1, and fetuin-A[20–23] are considered to play an important role in cardiovascular calcification, a dire complication of CKD. All these observations suggest that α-Kl and FGF23 are involved in the pathogeneses of not only aging-related syndromes, but also the complications of CKD. Thus, α-Kl, FGF23 and downstream molecules are candidate targets for therapeutic approaches aimed at ameliorating or delaying age-related syndromes and CKD complications.

Overproduction of 1,25(OH)2D[24] and subsequent altered mineral ion homeostasis, particularly severe hyperphosphatemia[25], are the major driving causes of tissue-damage phenotypes seen in α-*kl*$^{-/-}$and *Fgf23*$^{-/-}$ mice, as many of phenotypes of these mutant mice could be prevented by lowering of 1,25(OH)2D activity by (i) dietary restriction (a regimen in which α-*kl*$^{-/-}$ mice are fed a vitamin D-deficient diet)[3], or (ii) genetic ablation of *Cyp27b1* in α-*kl*$^{-/-}$mice or in *Fgf23*$^{-/-}$ mice[4,5], and the normalization of phosphate levels by (iii) genetic ablation of NaPi-IIa gene in α-*kl*$^{-/-}$ mice[26]. Induction of apoptosis by highly activated vitamin D was also studied in prostate and breast cancer cells[27–29]; these observations were further supported by the evidence that excessive activation of the vitamin D receptor (VDR) causes transcription of genes associated with mitochondrial export of cytochrome c and subsequent cleavage of caspase-9 and caspase-3, which promotes DNA fragmentation causing apoptosis[30]. Furthermore, Medici et al suggested a dual role of α-Kl and FGF23 in suppression of apoptotic actions of vitamin D through both negative regulation of 1α-hydroxylase expression and phosphoinositide-3 kinase- dependent inhibition of caspase activity[31].

Since marked activation of calpain-1 (μ-calpain) is detected in α-*kl*$^{-/-}$ mice[32], we believe that uncontrolled activation of calpain-1 could be associated with some of the age-associated phenotypes observed in α-*kl*$^{-/-}$ mice. Calpain is a calcium-dependent cytosolic cysteine protease, and two types of isozymic calpain, calpain-1 and calpain-2 are ubiquitously distributed in mammalian cells; the former is activated by micromolar concentrations of calcium and the latter is activated by millimolar concentrations of calcium. Calpain 1 is involved in many physiological and pathological processes by mediating proteolysis of various cellular proteins, including cytoskeletal proteins[33,34]. Of importance, calpain-1 over-activation causes irreversible cell damage and contributes to the pathology of cerebral and cardiac ischemia, Alzheimer's disease, arthritis, and cataract formation[35,36]. In this study, we tested whether hyperactivation of calpain-1 is responsible for the age-associated tissue damages of α-*kl*$^{-/-}$ mice, by evaluating the effect of BDA-410 (Fig. 1a), a relatively selective inhibitor of calpain-1 (Ki value of 130 nM) rather than calpain-2 (Ki value of 630 nM). We found that daily administration of BDA-410 greatly ameliorates most of the aging-related phenotypes that develop in α-*kl*$^{-/-}$ mice[3–5]. Taking into the consideration of the results of our study, we propose that modulation of calpain-1 activity is a potential therapeutic target for drug development towards delaying onsets of aging related syndromes caused by the abnormality of mineral homeostasis, and reducing the complications of CKD.

Results

Strategies for BDA-410 administration. We have shown that calpain-1 begins to be activated at 2 weeks of age in α-*kl*$^{-/-}$ mice, and at this stage, α-II-spectrin, a critical cytoskeletal target of

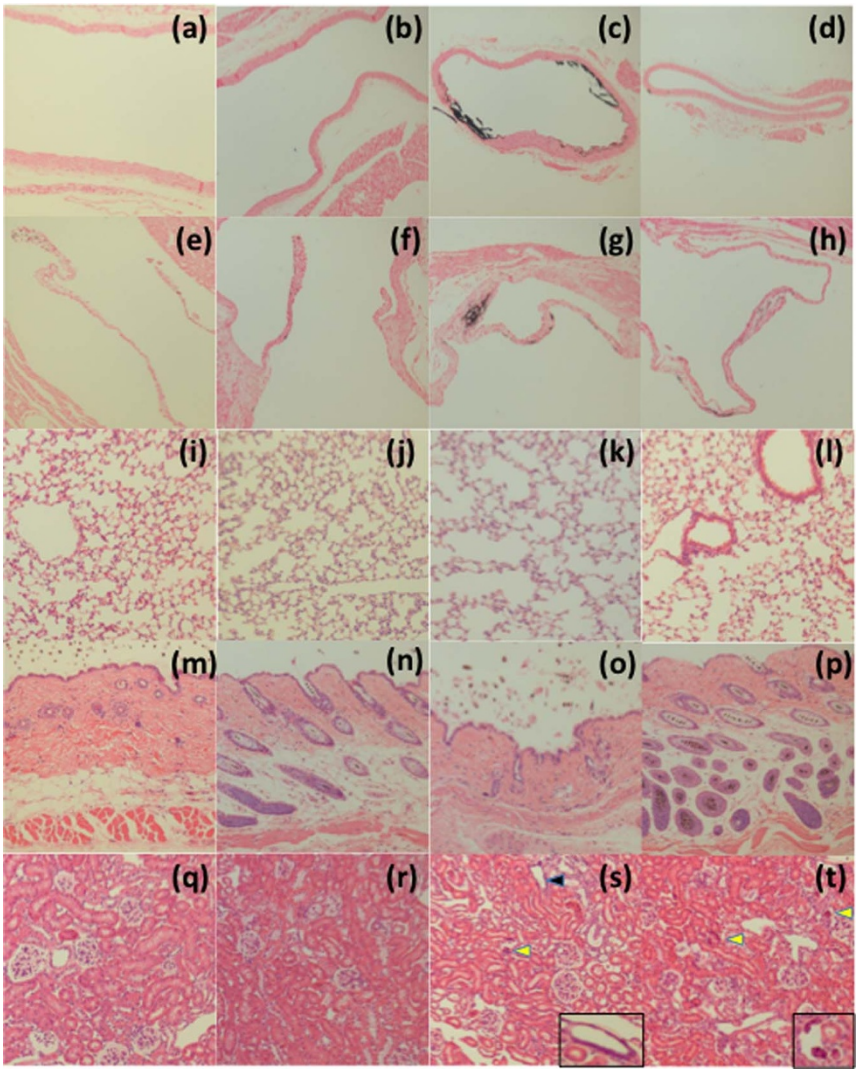

Figure 2 | The effects of BDA-410 administration on histological phenotypes. 3 μm sections of kidney, lung, heart, aorta and skin of wild and α-*kl*$^{-/-}$ mice given either BDA-410 or vehicle were stained with hematoxylin and eosin, or von Kossa. von Kossa staining sections of aortas from (a) wild type (vehicle) (N-2), (b) wild-type (BDA-410) (N=2), (c) α-*kl*$^{-/-}$(Vehicle) (N=2) and (d) α-*kl*$^{-/-}$(BDA-410) (N=3). Von Kossa staining sections of heart valves from (e) wild type (vehicle) (N-2), (f) wild-type (BDA-410) (N=2), (g) α-*kl*$^{-/-}$(Vehicle) (N=2) and (h) α-*kl*$^{-/-}$(BDA-410) (N=3). Hematoxylin and eosin staining sections of lung from (i) wild type (vehicle) (N=2), (j) wild-type (BDA-410) (N=2), (k) α-*kl*$^{-/-}$(Vehicle) (N-2) and (l) α-*kl*$^{-/-}$(BDA-410) (N=3). Hematoxylin and eosin staining sections of skin from (m) wild type (vehicle) (N=2), (n) wild-type (BDA-410) (N=2), (o) α-*kl*$^{-/-}$(Vehicle) (N-2) and (p) α-*kl*$^{-/-}$(BDA-410) (N=3). Hematoxylin and eosin staining sections of kidney from (q) wild type (vehicle) (N=2), (r) wild-type (BDA-410) (N=2), (s) α-*kl*$^{-/-}$(Vehicle) (insert indicates vascular calcification) (N-2) and (t) α-*kl*$^{-/-}$(BDA-410) (insert indicates calcification in tubule cells) (N=3). High resolution images are shown in supplementary Fig. 1.

calpain-1, remains almost intact. However, at 3 weeks of age, the abnormally activated calpain-1 has largely digested calpastatin, an endogenous calpain-1 inhibitor, and has started to cleave α-II-spectrin, resulting in cellular and tissue damage[31] (Fig. 1b). This might be the reason why tissue abnormalities become detectable in α-*kl*$^{-/-}$ mice from 3 weeks onwards. These findings are consistent with the idea that calpain-1 activation is a major and direct cause of tissue damage seen in α-*kl*$^{-/-}$ mice. Thus, we started intra-peritoneal injections of BDA-410 in α-*kl*$^{-/-}$ mice at 15 days or 28 days of age, before and after the appearance of the characteristic phenotypes, respectively, and continued them until 42 days (Fig. 1b). Based on the manufacturer's recommendation (BDA-410 dose: 30 mg to 100 mg/kg/day), we used doses of 25 mg, 50 mg and 100 mg/kg/day to examine the dose-response relationship. As expected, the lowest dose (25 mg/kg/day) of BDA-410 showed relatively less protective effect. However, α-*kl*$^{-/-}$ mice in the higher dose groups (50 mg, 100 mg/kg/day) showed recovery of growth almost to wild-type levels (Fig. 1d and e). Body weight gain, gross appearance, marked kyphosis and rough hair seen in α-*kl*$^{-/-}$ mice were all greatly ameliorated by BDA-410 treatment (Fig. 1c, e). Thus, in this study, unless otherwise mentioned, we administrated 100 mg/kg/day of BDA-410 to α-*kl*$^{-/-}$ and wild type mice from 15 to 42 days of age. In agreement with earlier observations[1], we found no sex-dependent difference in the effects of BDA-410.

The effects of BDA-410 administration on histological phenotypes. Cardiovascular calcification in aorta was no longer detectable after BDA-410 administration (Fig. 2d). Calcification-associated thickening of vessel walls was also no longer apparent. Heart valve calcifications obviously observed in α-*kl*$^{-/-}$ mice were vastly improved (Fig. 2h) by the administration of BDA-410. Histological observations showed that BDA-410 administration prevented emphysematous changes of α-*kl*$^{-/-}$ mice, and greatly ameliorated both enlargement of the air spaces distal to terminal bronchioles and destruction of alveolar walls (Fig. 2i to 2l). Since α-*kl*$^{-/-}$ mice is a good model of emphysematous changes often seen in

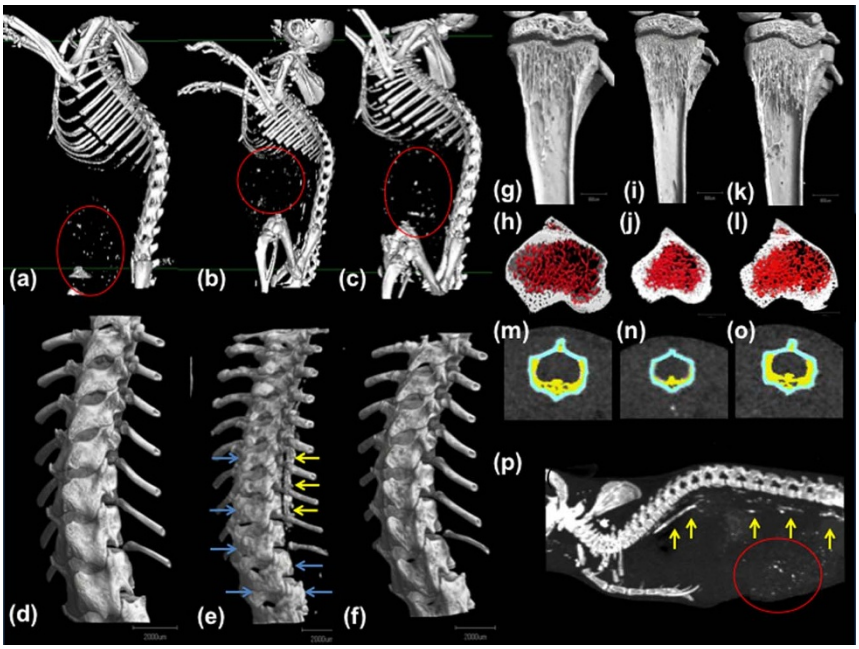

Figure 3 | μCT imaging of bones. Whole-body mouse CT images were obtained from wild type and α-*kl*$^{-/-}$ mice (N=2 each) which were treated with vehicle or BDA-410, respectively. Whole-body bones of wild-type (BDA-410) (a), α-*kl*$^{-/-}$(Vehicle) (b), and α-*kl*$^{-/-}$(BDA-410) (c). Spinal columns of wild-type (BDA-410) (d), α-*kl*$^{-/-}$(Vehicle) (e), and α-*kl*$^{-/-}$(BDA-410) (f). Tibiae of wild-type (BDA-410) (g, h), α-*kl*$^{-/-}$(Vehicle) (i, j), and α-*kl*$^{-/-}$(BDA-410) (k, l). Lumbar 1s of wild-type (BDA-410) (m), α-*kl*$^{-/-}$(Vehicle) (n), and α-*kl*$^{-/-}$(BDA-410) (o). Yellow arrows indicate ectopic calcifications in the aorta (e, p). Small calcium depositions enclosed by red circles are derived from fish bones that were provided in the diet. μCT imaging pictures of bones of vehicle treated wild-type mice are shown in supplementary Fig. 4.

aged populations[37], modulation of capain-1 activity might be a novel therapeutic target for pulmonary emphysema and chronic obstructive pulmonary disease (COPD). The characteristic features of skin aging in α-*kl*$^{-/-}$ mice include a reduced number of hair follicles with markedly atrophic dermal and epidermal thickness and barely detectable subcutaneous fat tissue, and such skin changes mimic senile atrophoderma in aged humans[38]. These abnormalities were markedly improved by BDA-410 treatment (Fig. 2p). Notably, hair follicles of wild and rescued skin (Fig. 2m, n and 2p) are possibly at second catagen phase, but that of mutant skin seems to be telogen phase (Fig. 2o). In B6 mice, the anagen phase of the second hair cycle starts at 20 to 23 days of age, transitions to catagen phase and enters the second telogen phase at around 42 days (lasting for 2 weeks), the day when mice were sacrificed. Since the hair cycle varies among individuals and also varies significantly from one skin region to another[39], we cannot yet reach a conclusion as to the effects of BDA-410 on the hair cycle. In the kidney section of vehicle treated α-*kl*$^{-/-}$ mice, we can detect two types of ectopic calcifications; vascular calcification (black arrow head) and the calcifications in the tubule cells (yellow arrow head) (Fig. 2s). It should be noted that although vascular calcification became largely undetectable after BDA-410 administration, tiny calcium precipitates were still detected in the cortical layer in nephron segments of α-*kl*$^{-/-}$ mice even after the administration of BDA-410 (Fig. 2t, Supplementary Fig. 2a). This type of tiny calcium precipitates were not detected in the kidney of *cyp27b1*$^{-/-}$/α-*kl*$^{-/-}$ mice[4] (1,25(OH)2D levels are lower than wild mice) and *NaPi2a*$^{-/-}$/α-*kl*$^{-/-}$ mice[26] fed with normal Pi diet (Pi levels are lower than in wild-type mice) (Supplementary Fig. 2c and e), but became detectable if *NaPi2a*$^{-/-}$/α-*kl*$^{-/-}$ mice were switched to a high Pi diet[26], indicating that the overproduction of $1,25(OH)_2D$, possibly together with the increase in Pi, is necessary for accumulation of calcium precipitates in the cortical layer of the kidney in α-*kl*$^{-/-}$mice. These suggest that tiny calcium precipitates are caused by a different mechanism from that of vascular calcification and so we discussed possible mechanism in the figure legend of supplementary Fig. 3.

μCT imaging clearly showed the characteristic bone phenotypes of α-*kl*$^{-/-}$ mice, such as a generalized decrease in bone mineral density, significantly reduced trabecular and cortical thickness, lower trabecular and cortical bone volume and a severely reduced trabecular bone fraction (Fig. 3b, e, i, j, n). All these phenotypes were improved closed to wild-type levels by BDA-410 administration (Fig. 3c, f, k, l, o). Furthermore, malformation of spongy bone (Fig. 3n), structural deformities of bones and irregular/rough appearances of bones (Fig. 3e, blue arrows) seen in α-*kl*$^{-/-}$ mice were ameliorated by BDA-410 administration (Fig. 3o, f). Ectopic calcification in the aorta of α-*kl*$^{-/-}$ mice (Fig. 3e, p; yellow arrows) was no longer detectable in BDA-410-treated animals (Fig. 3f).

Concomitantly with the above effects, the atrophic changes of organs (testis, ovary, uterus, and thymus, and external appearance of genital organs of both sexes) in α-*kl*$^{-/-}$ mice were all ameliorated in proportion to the recovery of whole-body size and weight in BDA-410 treated animals. Sperm in the testis (Supplementary Fig. 5f) and some ovarian follicles (Supplementary Fig. 6) appeared mature, and indeed, mating of rescued α-*kl*$^{-/-}$ male and female mice resulted in viable offspring (although the efficiency seems to be very low). However, we did not examine the effect of BDA-410 on the life-span of α-*kl*$^{-/-}$ mice, as prolonged daily intra-peritoneal injection of BDA-410 would be too stressful for the animals for such long-term study. Instead, to further study the effects of BDA-410, we started intra-peritoneal injections of BDA-410 at 28 days of age and confirmed that administration of BDA-410 is effective even after the appearance of characteristic histological phenotypes of α-*kl*$^{-/-}$ mice (Supplementary Fig. 5).

The effects of BDA-410 on serological phenotypes. We next analyzed the effects of BDA-410 administration on the serum levels of 1,25(OH)2D, Pi and Ca^{2+} to confirm that the activation of calpain-1 is the down-stream event of the overproduction of 1,25(OH)2D and subsequent altered mineral-ion metabolism. As expected, serum levels of 1,25(OH)2D, Pi and Ca^{2+} in α-*kl*$^{-/-}$ mice were not affected by the administration of BDA-410, and

1,25(OH)2D and, Pi were still significantly higher than those of wild type mice, indicating that calpain-1 is likely activated down-stream of $1,25(OH)_2D$ and hyperphosphatemia (Fig. 4a, b and c).

FGF23 expression in calcified arteries. We also found that serum FGF23 concentrations in α-*kl*$^{-/-}$ mice were not reduced by administration of BDA-410 and remained much higher than those of wild-type mice (Fig. 4d and e, lane 3). We then examined whether FGF23, usually expressed in osteocytes, was ectopically expressed in calcified arteries, since there is evidence that cardiovascular calcification is an active process that recapitulates regulated osteogenesis[40,41]. As shown in Fig. 4 and supplementary Fig. 7, FGF23, osteogenesis-related genes, Runx2, Osteopontin, and RANKL, were ectopically expressed in the aortas of 42-day-old α-*kl*$^{-/-}$ mice (lane 2). However, they were not detected when ectopic calcification was blocked by administration of BDA-410 (lane 3). Consistently with this result, expression of these genes was not detected in aortas from 17-day-old α-*kl*$^{-/-}$ mice (prior to the occurrence of cardio-vascular calcification) (lane 5), suggesting that the ectopic expressions of FGF23 are induced at the calcified arteries in parallel with the progression of cardiovascular calcification.

Discussion

Calpains are at the crossroads between physiological and pathological cellular activities[33,34]. Controlled calpain activation plays key roles in a variety of signaling processes, whereas abnormal calpain activation, in turn, results in uncontrolled degradation of the cellular protein pool, including signaling proteins, transcription factors, and cytoskeletal substrates[33,34]. It has been reported that $1,25(OH)_2D_3$ administration induces Ca^{2+}-mediated apoptosis in adipocytes and breast cancer cells via increased calcium influx and subsequent activation of calpain-1 and caspase-12[42,43]. In this study, we also found that abnormal activation of calpain-1 and consequent tissue damages are induced downstream of increased activity of vitamin D. Therefore, we speculated that overproduction of $1,25(OH)_2D$ disrupts physiological processes that regulate calpain-1 activity, leading to dysregulation of the cellular protein pool. In consequence of degradation of the cellular protein pool, tissue damage occurs in excess of the tissue-recovery capacity, resulting in failure to maintain cellular and tissue integrity (Supplementary Fig. 8). In this scenario, activation of calpain-1 can be seen as a key cellular event in α-*kl*$^{-/-}$ mice, leading to the appearance of the characteristic multiple aging-related phenotypes in these mice. Therefore, modulation of calpain-1 activity may prove useful in the alleviation of aging-related syndromes. However, at this stage, there are potential limitations associated with therapeutic use of calpain inhibitors; firstly, calpain family members are involved in a multiple physiological functions throughout life and, secondly, the active centers of calpain family members are highly conserved and similarly activated[33,34]. Therefore, multiple physiological functions of calpains might be affected by a single inhibitor. But, if we look at the calpain system from a different perspective, calpains are likely to cleave polypeptides at limited sites and to have regulatory or signaling functions in cells rather than digestive functions like those of lysosomal proteases, so undesired side effects of calpain inhibitors might be limited[35,36]. In fact, we could not detect any obvious side effects of BDA-410 in the histological samples of lung, kidney and liver prepared from wild-type mice to which we administrated BDA-410 (100 mg/kg/day) for 4 weeks, and this is consistent with the earlier findings of Trinchese et al[44]. Investigators, however, realize that 4 weeks of daily administrations might not be long enough to induce side-effects; for therapeutic use, it would be desirable to employ tissue-, cell- and/or target-calpain type-specific inhibition to minimize unexpected side effects in aging-related diseases or to ameliorate complications of patients with CKD.

Similar to those observed in α-*kl*$^{-/-}$ mice, activation of Calapin 1 occurred in aged wild type mice. As normal mice aged from 4 weeks to 29 months, the expression of α-Kl protein decreased, the activation of calpain 1 increased, the level of calpastatin considerably decreased, and the degradation of α-II-spectrin increased[32]. In addition, the expression of α-*kl* gene was gradually reduced in the rat

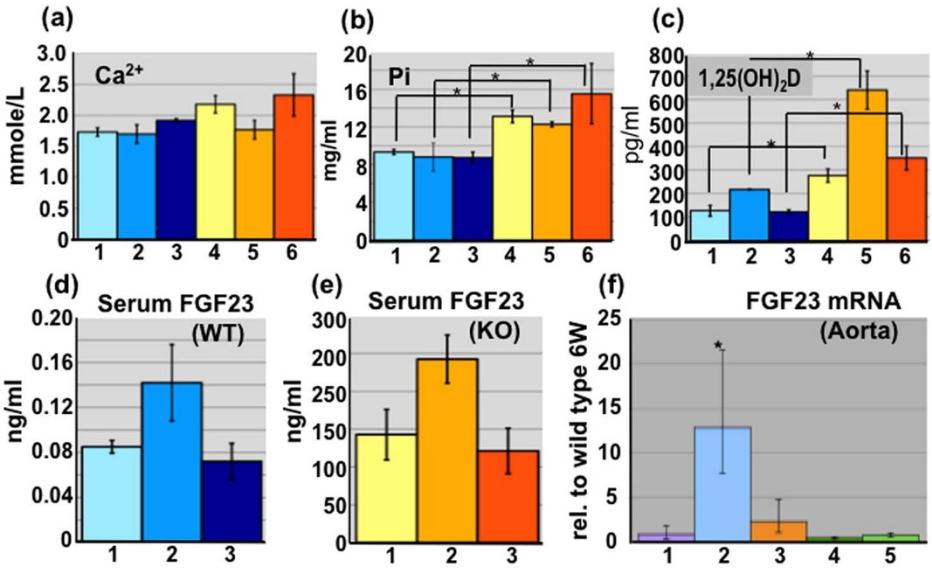

Figure 4 | Serological phenotypes and characterization of ectopic calcification. Serum levels of Ca^{2+} (a), Pi (b), and $1,25(OH)_2D$ (c) are indicated. Lane 1; 42-day-old wild-type (n=3), Lane 2; 17-day-old wild-type (n=2), Lane 3; 42-day-old wild-type (BDA-410 treated) (n=3). Lane 4; 42-day-old α-*kl*$^{-/-}$ (n=5), Lane 5; 17-day-old α-*kl*$^{-/-}$ (n=3), Lane 6; 42-day-old α-*kl*$^{-/-}$(BDA-410 treated) (n=4). Significant differences are indicated by asterisks* ($P \leqq 0.05$). Serum FGF23 levels in wild-type mice are indicated in (d). Lane 1; 42-day-old (n=5), Lane 2; 17-day-old (n=3), Lane 3; 42-day-old (BDA-410) (n=4). Serum FGF23 levels in α-*kl*$^{-/-}$ mice are indicated in (e). Lane 1; 42-day-old (n=5), Lane 2; 17-day-old (n=3), Lane 3; 42-day-old (BDA-410) (n=5). Gene expressions of Fgf23 are shown in (f). Lane 1; 42-day-old wild-type mice (N=3), Lane 2; 42-day-old α-*kl*$^{-/-}$ (N=3), lane 3; 42-day-old α-*kl*$^{-/-}$(BDA-410) (N=3), Lane 4; 17-day-old wild-type (N=3), Lane 5; 17-day-old α-*kl*$^{-/-}$(N=3). Expression levels were compared with the standard (Lane 1) and significant differences are indicated by asterisks* ($P \leqq 0.05$).

kidney during long term hypertension and the expression of α-*kl* mRNA and the production of α-Kl protein were severely reduced in CKD patients who develop multiple complications resembling phenotypes observed in α-*kl*$^{-/-}$ mice[10–14]. The above observations allow us to speculate that tissue deterioration during aging might be caused by a decrease of α-Kl protein, which leads to a decrease of calpastatin and activation of calpain 1, resulting in an enhanced degradation of cytoskeletal components such as spectrin. However, we could not examine the long-term beneficial effects of BDA-410 on tissue deterioration of aged wild type mice, as prolonging the daily intra-peritoneal injection of BDA-410 would be too stressful for the mice and technically is not a viable option.

A growing body of evidence indicates that increased plasma levels of FGF23 are closely associated with the high cardiovascular mortality, particularly in later to end stage CKD patients[45,46]. Our present findings might support these clinical observations. In fact, FGF23 is ectopically induced in the calcified arteries and thus at least partly mirrors the progression of the cardiovascular calcification, one of the major risk factors for cardiovascular mortality. This might be the reason why plasma levels of FGF23 are highlighted as the most correlated bio-marker for cardiovascular mortality, particularly in later- to end-stage CKD patients[45,46].

Here, we found that the uncontrolled activation of calpain-1 causes most of the α-*kl* deficient phenotypes and daily administration of BDA410, a calpain-1 inhibitor strikingly ameliorates such phenotypes of α-*kl*$^{-/-}$ mice. Further studies of the role of calpain-1 activation in the appearance of α-*kl*$^{-/-}$ phenotypes may help to identify further potential targets for intervention to prevent or delay the occurrence of ageing-related syndromes caused by dysregulation of mineral homeostasis and complications in advanced-stage CKD patients. In addition, hyperphosphatemia, the major cause of phenotypes of α-*kl*$^{-/-}$ mice[26], has been reported to be closely associated with high levels of cardiovascular disease morbidity and mortality in patients with CKD[16–19]. Therefore, it is also likely that some of the adverse effects of phosphate toxicity in patients with CKD might be ameliorated by selectively targeting calpain-1 activities.

Methods

Animals and Diets α-*kl*$^{-/-}$ mice were previously generated by conventional gene knock-out in our laboratory[3]. We cross-bred heterozygous α-*kl* and *cyp27b1* mice[47] to obtain compound heterozygous animals which were then interbred to generate the desired double homozygous mutants (*cyp27b1*$^{-/-}$/α-*kl*$^{-/-}$). Routine PCR using genomic DNA extracted from tail clips was performed for genotyping. Mice were housed in a barrier facility and maintained under specific pathogen-free conditions during the entire study period. α-*kl*$^{-/-}$ mice were fed ad libitum a standard diet containing 1.2% calcium, 0.8% phosphorus, and 6.4 IU/g vitamin D3 (CRF-1, Oriental Yeast Co. Ltd) and *cyp27b1*$^{-/-}$/α-*kl*$^{-/-}$ mice were fed ad libitum a high calcium/lactose diet 5A5L (Test Diet Co. Ltd.). All experimental procedures using laboratory animals were approved by the Animal Care and Use Committees of the Center for Developmental Biology, Riken (Riken CDB) and the Foundation for Biomedical Research and Innovation (FBRI). Efforts were made to minimize the number of animals used and their suffering. Animals were maintained in accordance with the Guides of RIKEN CDB and FBRI for the Care and Use of Laboratory Animals and all experiments used protocols approved by the institutions' subcommittees on animal care.

Generation of the double-homozygous mutants of *NaPi2a* and α-*kl* genes, genotyping and animal feeding conditions were described previously[26]. Mice were maintained in accordance with the NIH Guide for the Care and Use of Laboratory Animals, and experiments used protocols approved by the institutional subcommittee on animal care. All studies performed were approved by the Harvard Medical School Institutional Animal Care and Use Committee (Boston, MA, USA).

Protease inhibitor; BDA-410. BDA-410 was kindly provided by Mitsubishi Tanabe Pharma Corporation, Tokyo, Japan. The chemical name of this compound is (2S)-N-{(1S)-1-[(S)-hydroxy(3-oxo-2-phenyl-1-cyclopropen-1-yl)methyl]-2-methylpropyl}-2-benzenesulfonyl-amino-4-methylpentanamide (C_{26} H_{32} N_2 O_5 S, MW 484.61). The IC_{50} values for inhibition of papain (400 nM), cathepsin B (16 μM), cathepsin D (91.2 μM), cathepsin G (>100 μM), thrombin (>100 μM), and proteasome 20S (>100 μM) suggest the potential utility of BDA-410 as an inhibitor of cysteine proteases[48]. In addition to these *in vitro* studies, BDA-410 has been evaluated as a therapeutic modality to protect against neuronal cell death in models of Alzheimer's disease[44] and as a potential therapeutic agent for blood stage malaria, sickle cell disease, and angiotensin II induced abdominal aortic aneurysms and atherosclerosis[49,50].

Administration of BDA-410. Just before injection, BDA-410 was dissolved in a small amount of DMSO (20-50 μl) and diluted to the final concentration of 20 mg/ml by the addition of sesame oil. The BDA-410 solution was vigorously mixed and intraperitoneally injected into mice (25, 50, 100 mg/kg body weight) once per day from 15 to 42 or from 28 to 42 days of age.

Gross phenotype and body weight. The body weight of mice was measured every two days, usually starting at 15 days of age until 42 days. Overall bone structure, bone mineral densities, and ectopic calcifications in aorta were visualized by whole-body μ-CT scanning.

micro-CT scanning. Whole-body mouse CT images were obtained using a Latheta LCT200 (Hitachi Aloka Medical) according to the manufacturer's protocol. Mouse vertebrae and tibia bones were scanned using a SCANXMATE-E090S scanner (Comscantechno) at a tube voltage peak of 60 kVp and a tube current of 100 μA. Samples were rotated 360° in steps of 0.36°, generating 1,000 projection images of 640 × 480 pixels. The μ-CT data were reconstructed at an isotropic resolution of 9.5 × 9.5 × 9.5 μm^3. Three-dimensional tomographic images were obtained using TRI/3D-BON (RATOC Systems) or OsiriX (www.osirix-viewer.com) software.

Measurement of serum phosphate, calcium, 1,25(OH)$_2$D and FGF23. Mice were anesthetized with isoflavane. Blood was drawn from heart ventricles by puncture with a needle. Serum was isolated by centrifugation at 3000 × g for 10 min and stored at −30°C. Serum phosphorus and calcium were determined at SRL Inc. Japan using standard clinical methods. Serum levels of 1,25-(OH)$_2$D and FGF23 were measured by means of RIA (SRL Inc., Tokyo, Japan) and an ELISA system (SRL Inc., Tokyo, Japan), respectively.

Histological analyses. Wild and α-*kl*$^{-/-}$ mice given either BDA-410 or vehicle (control) were fixed with 4% paraformaldehyde or 10% buffered formalin. Kidney, liver, lung, heart aorta, skin, small intestine, ovary, and testis were subsequently embedded in paraffin. Paraffin sections (3 μm) of the above tissues were mounted on SuperFrost Plus glass slides. Sections were stained with hematoxylin and eosin, and von Kossa (incubated in 5% silver nitrate for 20 min under UV light irradiation) to visualize ectopic calcifications in various soft tissues. Histological examinations of *NaPi2a* and α-*kl* double knockout mice were described previously[26].

Immuno-staining. Frozen sections of kidney were mounted on SuperFrost Plus glass slides and incubated with primary antibody (monoclonal antibodies against Calbindin D28K (diluted 1 : 200, abcam ab 11426) and anti-β-galactosidase (diluted 1 : 1000, abcam ab936)) overnight at 4°C. They were then incubated with the secondary antibodies (goat anti-rabbit IgG (diluted 1 : 1000, CF594, BIOTIUM) and goat anti-chicken IgY (diluted 1 : 1000, CF488, BIOTIUM) respectively, at room temperature for 3 to 4 hours.

Quantitative real-time PCR. Total RNA fractions isolated from aorta of wild and α-*kl*$^{-/-}$ mice given either BDA-410 or vehicle (control) were used for evaluation of relative expression levels of FGF23, Runx2, Ostopontin, and RANKL as described earlier[4,5]. For real-time polymerase chain reaction (PCR), 10 μL (corresponding to approximately 50 ng of RNA) of each first-strand reaction product was amplified with appropriate primers and the corresponding fluorescent probes for FGF23 (assay IDs: Mm00445621-m1), Runx (assay IDs: M0m0501584-m1), Osteopontin (assay IDs: Mm00436767-m1), RANKL (assay IDs: Mm00441906-ml), and 18S RNA (439413E). The probes were designed using the "Assay-on-Demand" service of Applied Biosystems (Forster City, CA). Real-time PCR was performed in duplicate, and all the reactions were suitably controlled (no-template control and standard positive control). The quantity of mRNA was calculated by normalizing the C_T (threshold cycle value) of FGF23 to the C_T of 18S RNA of the same RNA sample, as follows: the average 18S RNA C_T value (each multiplex PCR was done in duplicate) was subtracted from the average FGF23 C_T value, and this result was taken as ΔC_T. This ΔC_T is specific and can be compared with the ΔCT of a control calibration sample. The value obtained by subtraction of control ΔC_T from the ΔC_T of FGF23 is referred as $\Delta\Delta C_T$. The relative expression level of FGF23, Runx, Osteopontin or RANKL (in comparison to the vehicle control) in aorta isolated from wild and α-*kl*$^{-/-}$ mice given either BDA-410 or vehicle (control) was determined as 2-$\Delta\Delta C_T$.

Statistical methods. Statistically significant differences between groups were evaluated by means of Student's *t* test for comparison between 2 groups. All values are expressed as means ± SE. All analyses were performed using Microsoft Excel (Microsoft, Redmond, WA, USA).

1. Kuro-o, M. *et al*. Mutation of the mouse *Klotho* gene leads to a syndrome resembling ageing. *Nature* **390**, 45–51 (1997).
2. Yoshida, T., Fujimori, T. & Nabeshima, Y. Mediation of unusually high concentrations of 1,25-dihydroxyvitamin D3 in homozygous klotho mutant mice by increased expression of renal 1alpha-hydroxylase gene. *Endocrinology* **143**, 683–689 (2002).
3. Tsujikawa, H., Kurotaki, Y., Fujimori, T., Fukuda, K. & Nabeshima, Y. Klotho, a gene related to a syndrome resembling human premature aging, functions in a negative regulatory circuit of vitamin D endocrine system. *Mol. Endocrinol.* **17**, 2393–2403 (2003).

4. Ohnishi, M., Nakatani, T., Lanske, B. & Razzaque, M. S. Reversal of mineral ion homeostasis and soft-tissue calcification of klotho knockout mice by deletion of vitamin D 1α-hydroxylase. *Kidney Int.* **75**, 1166–1172 (2006).
5. Razzaque, M. S., Sitara, D., Taguchi, T., St-Arnaud, R. & Lanske, B. Premature aging-like phenotype in fibroblast growth factor 23 null mice is a vitamin D mediated process. *FASEB J.* **20**, 720–722 (2006).
6. Nakatani, T. *et al.* In vivo genetic evidence for klotho-dependent, fibroblast growth factor 23 (Fgf23) -mediated regulation of systemic phosphate homeostasis. *FASEB J.* **23**, 433–41 (2009).
7. Urakawa, I. *et al.* Klotho converts canonical FGF receptor into a specific receptor for FGF23. *Nature* **444**, 770–774 (2006).
8. Bhattacharyya, N., Chong, W. H., Gafni, R. I. & Collins, M. T. Fibroblast growth factor 23: state of the field and future directions. *Trends in Endocrinology & Metabolism* **23**, 610–618 (2012).
9. Kovesdy, C. P. & Quarles, L. D. Fibroblast growth factor-23: what we know, what we don't know, and what we need to know. *Nephrol. Dial. Transplant.* Apr 25 (2013).
10. London, G. M. & Drueke, T. B. Atherosclerosis and arteriosclerosis in chronic renal failure. *Kidney Int.* **51**, 1678–1695 (1997).
11. Rostand, S. G. & Drueke, T. B. Parathyroid hormone, vitamin D, and cardiovascular disease in chronic renal failure. *Kidney Int.* **56**, 383–392 (1999).
12. Milliner, D. S., Zinsmeister, A. R., Lieberman, E. & Landing, B. Soft tissue calcification in pediatric patients with end-stage renal disease. *Kidney Int.* **38**, 931–936 (1990).
13. Urena, P. & De Vernejoul, M. C. Circulating biochemical markers of bone remodeling in uremic patients. *Kidney Int.* **55**, 2141–2156 (1999).
14. Kuizon, B. D. & Salusky, I. B. Growth retardation in children with chronic renal failure. *J. Bone Miner. Res.* **14**, 1680–1690 (1999).
15. Koh, N. *et al.* Severely reduced expression of Klotho gene in human chronic renal failure kidney. *Biochem. Biophys. Res. Commun.* **280**, 1015–1020 (2001).
16. Mathew, S., Tustison, K. S., Sugatani, T., Chaudhary, L. R., Rifas, L. & Hruska, K. A. The mechanism of phosphorus as a cardiovascular risk factor in CKD. *J. Am. Soc. Nephrol.* **19**, 1092–1105 (2008).
17. Komaba, H. & Fukagawa, M. The role of FGF23 in CKD--with or without Klotho. *Nat. Rev. Nephrol.* **8**, 484–90 (2012).
18. Quarles, L. D. Role of FGF23 in vitamin D and phosphate metabolism: implications in chronic kidney disease. *Exp. Cell Res.* **318**, 1040–1048 (2012).
19. Stubbs, J. R. *et al.* Role of hyperphosphatemia and 1,25-dihydroxyvitamin D in vascular calcification and mortality in fibroblastic growth factor 23 null mice. *J Am Soc Nephrol* **18**, 2116–2124 (2007).
20. Wallin, R., Wajih, N., Greenwood, G. T. & Sane, D. C. Arterial calcification: A review of mechanisms, animal models, and the prospects for therapy. *Med Res Rev* **21**, 274–301 (2001).
21. Proudfoot, D. & Shanahan, C. M. Molecular mechanisms mediating vascular calcification: Role of matrix Gla protein. *Nephrology* **11**, 455–461 (2006).
22. Moe, S. M. *et al.* Role of calcification inhibitors in the pathogenesis of vascular calcification in chronic kidney disease (CKD). *Kidney Int.* **67**, 2295–2304 (2005).
23. Mellgren, R. L. & Huang, X. Fetuin A stabilizes m-calpain and facilitates plasma membrane repair. *J Biol Chem* **282**, 35868–35877 (2007).
24. Razzaque, M. S. & Lanske, B. Hypervitaminosis D and premature aging: lessons learned from Fgf23 and Klotho mutant mice. *Trends Mol Med.* **12**, 298–305 (2006).
25. Razzaque, M. S. Phosphate toxicity: new insights into an old problem. *Clin Sci (Lond).* **120**, 91–7 (2011).
26. Ohnishi, M. & Razzaque, M. S. Dietary and genetic evidence for phosphate toxicity accelerating mammalian aging. *FASEB J.* **24**, 3562–3571 (2010).
27. Narvaez, C. J., Zinser, G. & Welsh, J. Functions of 1α, 25-dihydroxyvitamin D3 in mammary gland: from normal development to breast cancer. *Steroids* **66**, 301–308 (2001).
28. Johnson, C. S., Hershberger, P. A. & Trump, D. L. Vitamin D-related therapies in prostate cancer. *Cancer Metastasis Rev.* **21**, 147–158 (2002).
29. Johnson, C. S., Muindi, J. R., Hershberger, P. A. & Trump, D. L. The antitumor efficacy of calcitriol: preclinical studies. *Anticancer Res.* **26**, 2543–2549 (2006).
30. Demay, M. B. Mechanism of vitamin D receptor action. *Ann. N. Y. Acad. Sci.* **1068**, 204–213 (2006).
31. Medici, D. *et al.* FGF-23-Klotho signaling stimulates proliferation and prevents vitamin D-induced apoptosis. *J. Cell Biol.* **182**, 459–465 (2008).
32. Manya, H., Fujimori, T., Nabeshima, Y. & Endo, T. Klotho protein deficiency leads to overactivation of (Mu)-calpain. *J. Biol. Chem.* **277**, 35503–35508 (2002).
33. Goll, D. E., Thompson, V. F., Li, H., Wei, W. & Cong, J. The calpain system. *Physiol. Rev.* **83**, 731–801 (2003).
34. Campbell, R. L. & Davies, P. L. Structure-function relationships in calpains. *Biochem. J.* **447**, 335–351 (2012).
35. Wang, K. K. & Yuen, P. W. Calpain inhibition: an overview of its therapeutic potential. *Trends Pharmacol. Sci.* **15**, 412–419 (1994).
36. Lee, M. S. *et al.* Neurotoxicity induces cleavage of p35 to p25 by calpain. *Nature* **405**, 360–364 (2000).
37. Sato, A. *et al.* Morphological mechanism of the development of pulmonary emphysema in klotho mice. *Proc. Natl. Acad. Sci. USA* **104**, 2361–2365 (2007).
38. Calleja-Agius, J., Muscat-Baron, Y. & Brincat, M. P. Skin ageing. *Menopause Int.* **13**, 60–64 (2007).
39. Alonso, L. & Fuchs, E. The hair cycle. *J. Cell Sci.* **119**, 391–393 (2006).
40. Sage, A. P., Tintut, Y. & Demer, L. L. Regulatory mechanisms in atherosclerotic calcification. *Nat. Rev. Cardiol.* **7**, 528–536 (2010).
41. Shao, J. S., Cheng, S. L., Sadhu, J. & Towler, D. A. Inflammation and the osteogenic regulation of vascular calcification: a review and perspective. *Hypertension* **55**, 579–592 (2010).
42. Sergeev, I. N. 1,25-Dihydroxyvitamin D3 induces Ca^{2+}-mediated apoptosis in adipocytes via activation of calpain and caspase-12. *Biochem. Biophys. Res. Commun.* **384**, 18–21 (2009).
43. Sergeev, I. N. Calcium signaling in cancer and vitamin D. *J. Steroid Biochem. Mol. Biol.* **97**, 145–151 (2005).
44. Trinchese, F. *et al.* Inhibition of calpains improves memory and synaptic transmission in a mouse model of Alzheimer disease. *J. Clin. Invest.* **118**, 2796–2807 (2008).
45. Isakova, T. *et al.* Chronic Renal Insufficiency Cohort Study Group: Fibroblast growth factor 23 is elevated before parathyroid hormone and phosphate in chronic kidney disease. *Kidney Int.* **79**, 1370–1378 (2011).
46. Kendrick, J. & Chonchol, M. The role of phosphorus in the development and progression of vascular calcification. *Am. J. Kidney Dis.* **58**, 826–834 (2011).
47. Dardenne, O., Prud'homme, J., Arabian, A., Glorieux, F. H. & St-Arnaud, R. Targeted inactivation of the 25-hydroxyvitamin D(3)-1(alpha)-hydroxylase gene (CYP27B1) creates an animal model of pseudovitamin D-deficiency rickets. *Endocrinology* **142**, 3135–3141 (2001).
48. Li, X., Chen, H., Jeong, J.-J., Athar, H. & Chishti, A. H. BDA-410: A novel synthetic calpain inhibitor active against blood stage malaria. *Mol. Biochem. Parasitol.* **155**, 26–32 (2007).
49. De Franceschi, L. *et al.* Pharmacological inhibition of calpain-1 prevents red cell dehydration and reduces Gardos channel activity in a mouse model of sickle cell disease. *FASEB J.* **27**, 750–759 (2013).
50. Subramanian, V. *et al.* Calpain inhibition attenuates angiotensin II-induced abdominal aortic aneurysms and atherosclerosis in low-density lipoprotein receptor-deficient mice. *J. Cardiovasc. Pharmacol.* **59**, 66–76 (2012).

Acknowledgments

We are grateful to all staff of the animal facility center RIKEN CDB, Dr. René St-Arnaud for supplying *cyp27b1*$^{-/-}$ mice, and Mitsubishi Tanabe Pharma Corporation Tokyo, Japan for supplying BDA-410. We thank K. Yurugi for technical assistance and Drs. T. Tsuruyama, T. Tanaka, R. Maeda, Y. Hashimoto, N. Nakamura, and K. Kobayashi for helpful suggestions and critical discussions. This work was supported by a grant-in-aid for Scientific Research (S) (22229003, to Y.N.) from the Ministry of Education, Culture, Sports, Science and Technology.

Author contributions

Y.N. performed most of the experiments on the effects of BDA-410 on aging phenotypes. M.W. analyzed gene expression, M.T., A.M. and T.S. studied bone mineral density by μCT scanning, M.O. and M.S.R. analyzed phenotypes of *NaPi2a*$^{-/-}$/*α-kl*$^{-/-}$ mice. M.S.R. critically read and edited the manuscript and provided insightful comments. H.I. analyzed *α-kl*$^{-/-}$/*cyp27b1*$^{-/-}$ mice. Y.-i. N. designed the experiments, supervised the project, provided funding and wrote the manuscript.

Additional information

Supplementary information accompanies this paper at http://www.nature.com/scientificreports

Competing financial interests: The authors declare no competing financial interests.

How to cite this article: Nabeshima, Y. *et al.* Calpain 1 inhibitor BDA-410 ameliorates *α-klotho*-deficiency phenotypes resembling human aging-related syndromes. *Sci. Rep.* **4**, 5847; DOI:10.1038/srep05847 (2014).